The exocyst is required for photoreceptor ciliogenesis and retinal development

Received for publication, May 10, 2017, and in revised form, July 10, 2017 Published, Papers in Press, July 20, 2017, DOI 10.1074/jbc.M117.795674

Glenn P. Lobo[‡§], Diana Fulmer[‡¶], Lilong Guo[‡¶], Xiaofeng Zuo[‡], Yujing Dang[‡], Seok-Hyung Kim[‡], Yanhui Su[‡], Kola George[‡], Elisabeth Obert[§], Ben Fogelgren[‖], Deepak Nihalani[‡], Russell A. Norris[¶], Bärbel Rohrer[§], and Joshua H. Lipschutz[‡ ‡‡1]**

*From the Departments of [‡]Medicine, [§]Ophthalmology, and [¶]Regenerative Medicine and Cell Biology, Medical University of South Carolina, Charleston, South Carolina 29425, the [‖]Department of Anatomy, Biochemistry, and Physiology, University of Hawaii at Manoa, Honolulu, Hawaii 96813, the **Division of Research, Ralph H. Johnson Veterans Affairs Medical Center, Charleston, South Carolina 29401, and the [‡‡]Department of Medicine, Ralph H. Johnson Veterans Affairs Medical Center, Charleston, South Carolina 29425*

Edited by Peter Cresswell

We previously have shown that the highly conserved eight-protein exocyst trafficking complex is required for ciliogenesis in kidney tubule cells. We hypothesized here that ciliogenic programs are conserved across organs and species. To determine whether renal primary ciliogenic programs are conserved in the eye, and to characterize the function and mechanisms by which the exocyst regulates eye development in zebrafish, we focused on *exoc5*, a central component of the exocyst complex, by analyzing both *exoc5* zebrafish mutants, and photoreceptor-specific Exoc5 knock-out mice. Two separate *exoc5* mutant zebrafish lines phenocopied *exoc5* morphants and, strikingly, exhibited a virtual absence of photoreceptors, along with abnormal retinal development and cell death. Because the zebrafish mutant was a global knockout, we also observed defects in several ciliated organs, including the brain (hydrocephalus), heart (cardiac edema), and kidney (disordered and shorter cilia). *exoc5* knockout increased phosphorylation of the regulatory protein Mob1, consistent with Hippo pathway activation. *exoc5* mutant zebrafish rescue with human EXOC5 mRNA completely reversed the mutant phenotype. We accomplished photoreceptor-specific knockout of Exoc5 with our *Exoc5* fl/fl mouse line crossed with a rhodopsin-Cre driver line. In *Exoc5* photoreceptor-specific knock-out mice, the photoreceptor outer segment structure was severely impaired at 4 weeks of age, although a full-field electroretinogram indicated a visual response was still present. However, by 6 weeks, visual responses were eliminated. In summary, we show that ciliogenesis programs are conserved in the kidneys and eyes of zebrafish and mice and that the exocyst is necessary for photoreceptor ciliogenesis and retinal development, most likely by trafficking cilia and outer-segment proteins.

Cilia are thin rod-like microtubule-based organelles, which are found on most mammalian cell types. Cilia can be classified as either motile or non-motile (more commonly referred to as primary) cilia. Motile cilia function mainly as motor organelles, and primary cilia are mainly sensory organelles (1–3). Dysfunction of primary cilia results in human disorders, termed ciliopathies. Ciliopathies, such as Bardet-Biedl, Joubert, Meckel-Gruber, and Senior-Loken syndromes, affect multiple organs, resulting in central nervous system malformation, cystic kidney disease, and retinal dystrophy (4–6). Zebrafish models for several ciliopathies, including *cep290, cc2d2a, inpp5e, ift57, ift88,* and *ift172,* have kidney and retina phenotypes that suggest a common mechanism underlying these defects (7–10). An open question is whether primary ciliogenic programs, such as exocyst-related ciliary trafficking, are conserved across organs and species. Here, we build on our previous data on exocyst-dependent renal ciliopathy and extend this to retinal ciliopathy, comparing zebrafish and mice.

The vertebrate retina is organized into three distinct laminae: the outer nuclear layer (ONL),[2] the inner nuclear layer (INL), and the ganglion cell layer. The photoreceptor cells in the ONL have a specialized morphology consisting of an inner and outer segment that is linked by a connecting cilium and are highly polarized and light-sensitive cells. The inner segment, where protein synthesis occurs, is connected by the cilium to the outer segment, which consists of a microtubule-based axoneme and membrane disc stacks containing opsin required for phototransduction (11–13). The photoreceptor outer segment is considered to be a modified cilium (12–14).

This work was supported in part by grants from the Veterans Affairs (Merit Award I01 BX000820 (to J. H. L.) and National Institutes of Health Grants P30DK074038 (to J. H. L.), R21EY025034 (to G. P. L.), R01HL131546 (to R. A. N.), P20GM103444 (to R. A. N.), and R01HL127692 (to R. A. N.). The authors declare that they have no conflicts of interest with the contents of this article. The content is solely the responsibility of the authors and does not necessarily represent the official views of the National Institutes of Health.

This article contains supplemental Figs. S1 and S2.

[1] Holds the Arthur V. Williams Chair. To whom correspondence should be addressed: Medical University of South Carolina, 96 Jonathan Lucas St., CSB 829, Charleston, SC 29425. Tel.: 843-792-7659; Fax: 843-792-8399; E-mail: lipschut@musc.edu.

[2] The abbreviations used are: ONL, outer nuclear layer; E, embryonic day; ERG, electroretinography; hpf, hours post-fertilization; INL, inner nuclear layer; MDCK, Madin-Darby canine kidney; P, postnatal; PKD, polycystic kidney disease; OPL, outer plexiform layer; RPE, retina pigmented epithelium; TEM, transmission electron microscopy; TGN, trans-Golgi network; dpf, days post-fertilized; BisTris, 2-[bis(2-hydroxyethyl)amino]-2-(hydroxymethyl)-propane-1,3-diol; ANOVA, analysis of variance; PNA, peanut agglutinin.

Zebrafish are vertebrates, and zebrafish eyes are well laminated structures that are functionally very similar to the eyes of other vertebrates, including humans. Eye morphogenesis in the zebrafish starts at 11.5 h post-fertilization (hpf), and the eyecup is well-formed by 24 hpf. By 48 hpf, most of the retina is subdivided into its characteristic sublaminae (14). The connecting cilia and basal body in the inner segment are observed at 50 hpf, and the outer segment is visible by 54 hpf. The first visual responses can be elicited around 70 hpf, and photoreceptor cells reach adult size by 576 hpf (24 days) (14, 15).

In mice, eye development begins at embryonic day 8 (E8), and evidence of retinal development is seen at E13.5. At about the same time, E13, rod photoreceptor cells can be observed, with the peak production of rod photoreceptors occurring at postnatal day 1 (P1). In contrast, cone photoreceptors are all generated between E12 and E18. At birth, these newly formed photoreceptor precursors occupy the distal half of the retina forming a mantle of poorly differentiated cells. By P10, the differentiating photoreceptors have migrated into the ONL, after which they start their final process of maturation, the growth of the outer segment, and the establishment of functional synapses within the outer plexiform layer (OPL). Formation of the OPL, a layer of synapses between dendrites of bipolar and horizontal cells from the inner nuclear layer, and photoreceptor terminal axons from the ONL, is complete by P14 (16).

All cells in the retina are ciliated; however, here we paid particular attention to photoreceptor cells. In photoreceptor cells, vesicles containing proteins that are destined for the outer segment traffic from the trans-Golgi network (TGN) to the base of the connecting cilium via vesicular transport (17–19). The connecting cilium therefore plays a critical role as the bridge between the inner and outer segments. One of the central proteins implicated in vesicular trafficking from the TGN to the cilium in photoreceptors is the small GTPase, Rab8 (20). Disruption of Rab8 in *Xenopus* photoreceptor cells blocks rhodopsin-bearing post-TGN vesicle trafficking and results in abnormal accumulation of rhodopsin carrier vesicles at the base of the connecting cilium. Rab proteins perform functions through downstream effectors, such as the exocyst, a highly conserved eight protein trafficking complex (17, 19).

We previously demonstrated that the exocyst is required for ciliogenesis in canine renal tubule cells, due to its role in targeting and docking vesicles carrying ciliary proteins (21). We also showed that Cdc42, another small GTPase, localizes the exocyst to the primary cilium and biochemically and genetically interacts with exocyst complex member Exoc5 (also known as Sec10) (22). Interestingly, we found in zebrafish, using antisense morpholinos, that knockdown of *exoc5* resulted in small eyes (23) and knockdown of *cdc42* led to small eyes and loss of photoreceptor cilia (24) and that *exoc5* and *cdc42* seemed to act synergistically in ocular and retinal development (25).

Here, we describe the role of *exoc5* in eye development using mutant *exoc5* zebrafish, photoreceptor-specific *Exoc5* mouse knockouts, histology, immunohistology, and transmission electron microscopy (TEM). These data show that there exists a conserved ciliogenic program across species and organs.

Results

Zebrafish exoc5 mutants exhibit a ciliopathy phenotype and activation of the Hippo pathway

We previously showed that antisense morpholino knockdown of *exoc5* (also known as *sec10*) in zebrafish is associated with ciliary defects, including upward tail curvature and cardiac malformations as well as smaller eyes and increased cell death in the retina, the latter suggesting that *exoc5* plays a critical role in retinal cell development and maintenance (23). Given the concerns about off-target effects of morpholinos in experiments designed to further characterize the physiologic role of *exoc5* in retinal cell development and homeostasis, we utilized an *exoc5* mutant zebrafish line from the Zebrafish International Resource Consortium (ZIRC), *exoc5* sa23168. By sequencing of the mutants, we first confirmed that a single point mutation (CGA→TGA) at codon 377 led to a premature stop codon (Fig. 1, *A* and *B*), which previously had been shown to result in a truncated (at amino acid 376) and non-functional Exoc5 protein. By light microscopy, we observed that the gross phenotype of *exoc5* mutants was similar to other zebrafish mutants or morphants with defects in cilia formation and function (26, 27). At 3.5 dpf, all *exoc5* mutants had an upward tail curvature, smaller eyes, pericardial edema, and hydrocephalus (Fig. 1, *D* and *F*), when compared with wild-type (WT) siblings (Fig. 1, *C* and *E*). The morphologic phenotype was consistently observed in ~25% of the progeny from crosses of heterozygous parents as would be expected for Mendelian inheritance of a recessive mutation, with *exoc5* mutants surviving to at least 4 dpf. By Western blot analysis, we confirmed that Exoc5 protein was undetectable in *exoc5* mutant larvae, when compared with their WT siblings (Fig. 1*G*).

The exocyst is thought to act as a holocomplex, and we previously showed that knockdown of Exoc5 in MDCK cells resulted in the disruption of the exocyst and loss of other exocyst complex members, most likely by degradation in the proteasome, as the exocyst complex disintegrates in the absence of Exoc5 (21). To confirm this observation *in vivo*, we probed for Exoc4 protein expression in the *exoc5* mutants. Wild-type 3.5 dpf larvae showed strong expression of Exoc4 protein. In contrast, knockout of *exoc5* resulted in significantly depleted levels of Exoc4 protein (Fig. 1*G*). Interestingly, knockout of *exoc5* resulted in an increase in Mob1 phosphorylation (pMOB1), consistent with activation of the Hippo pathway (Fig. 1, *G* and *H*), a pathway known to be involved in restraining organ growth (28, 29).

To confirm that the ciliary defects observed in *exoc5* mutants were caused specifically by loss of *exoc5*, we performed rescue experiments by injecting wild-type human *EXOC5* mRNA into control and *exoc5* mutant embryos at the 1–2-cell stage. At 3.5 dpf, we found that low dose (100 pg) reconstitution of *EXOC5* mRNA, in *exoc5* mutant embryos, partially rescues the heart and eye phenotype, whereas high dose (250 pg) *EXOC5* mRNA fully rescues the *exoc5* mutant phenotype (Fig. 1*I*). To ensure

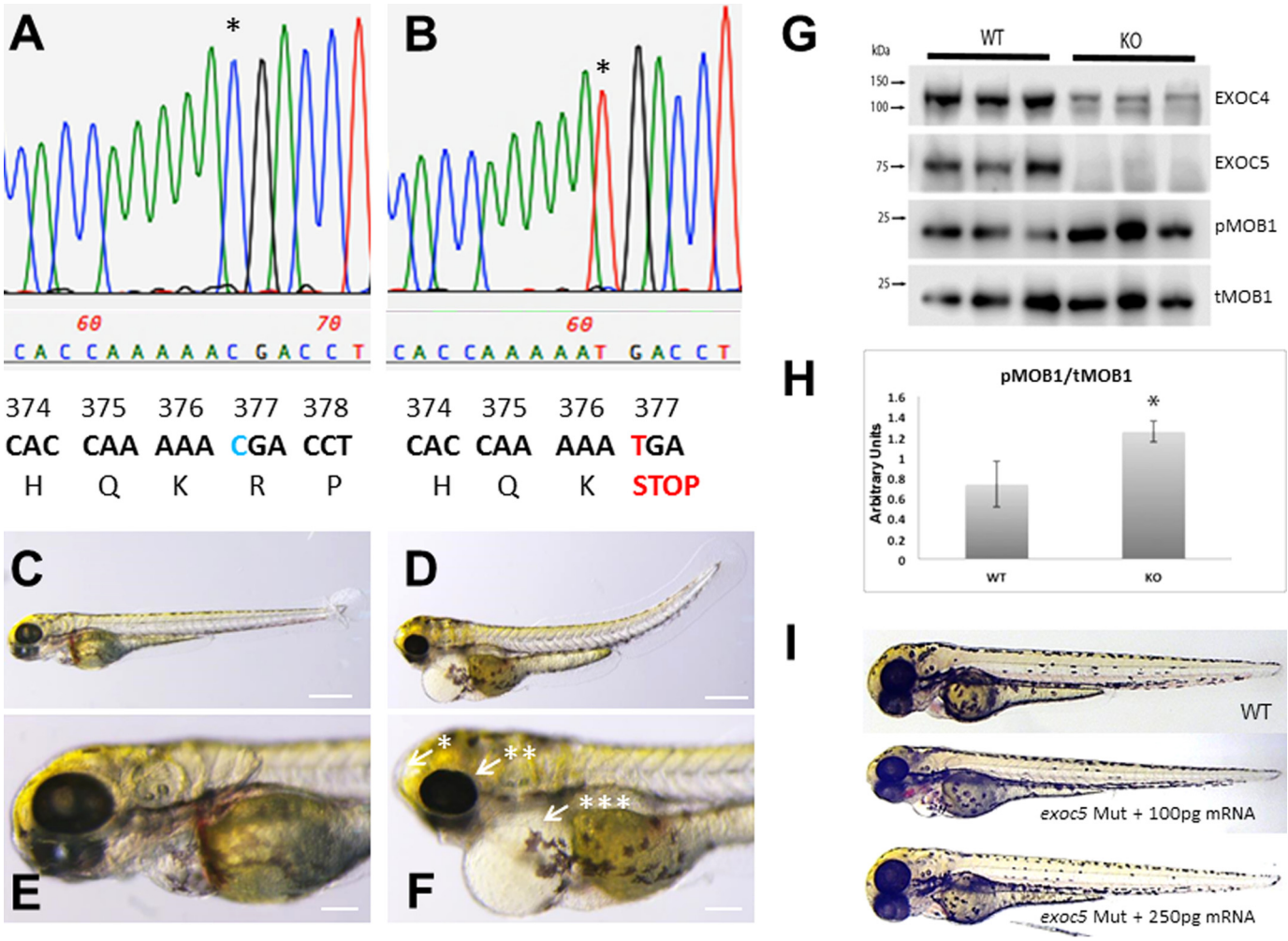

Figure 1. Exoc5 mutant zebrafish show ciliopathy phenotypes and up-regulation of the Hippo pathway. *A* and *B,* chromatograms of Sanger sequencing reactions of wild-type (*WT*) and homozygous *exoc5* mutant (*exoc5* Mut) zebrafish. *C–F,* lateral view of representative WT (*C* and *E*) and *exoc5* homozygous mutant (*D* and *F*) zebrafish at 3.5 dpf. *exoc5* mutants showed cilia defects, which included the following: *, hydrocephaly; **, smaller eyes; ***, pericardial edema and tail curvature. *Scale bars,* 0.268 mm (*C* and *D*) and 0.1 mm (*E* and *F*). *G,* Western blot analysis of WT and *exoc5* mutant zebrafish larvae. *Exoc5* mutants showed loss of Exoc5 and Exoc4 proteins and up-regulation of active phosphorylated mob1 (pMOB1) protein, at 3.5 dpf. Protein lysate was isolated from $n = 3$ zebrafish larvae, and all the protein lysate was loaded onto each gel lane. *H,* quantification of phosphorylated Mob1 protein in WT *versus exoc5* mutants (KO). $p = 0.023$. *I,* injection of wild-type human *EXOC5* mRNA rescues the *exoc5* mutant phenotype in zebrafish. This experiment was repeated twice, and a total of 120 rescued embryos were studied.

that the loss of *exoc5* was causing the phenotype, another *exoc5* mutant, using CRISPR gene editing, was generated, and the resulting phenotype was observed to be virtually identical to the *exoc5* mutant phenotype described above, as well as to our previously described *exoc5* morphants (supplemental Fig. 1) (23). These data show that loss of functional *Exoc5 protein* in zebrafish leads to gross pathology indicative of ciliopathy in the heart, brain, and eye.

Knockout of exoc5 in zebrafish results in early retinal phenotypes

Histologic analysis was completed to examine retinal morphology in *exoc5* mutant zebrafish larvae at 3.5 dpf. In transverse sections, all *exoc5* mutants exhibited smaller eyes and abnormal retinal lamination (Fig. 2, *A* and *B*). Interestingly, the photoreceptor/ONL layer in *exoc5* mutants was incompletely formed and severely disorganized (Fig. 2, *A* and *B*). Disorganization and lack of photoreceptor outer segments was more obvious by TEM of *exoc5* mutant larvae at 3.5 dpf. In WT siblings, cone photoreceptor outer segments extended toward the retina pigmented epithelium (RPE) in a parallel and organized manner and exhibited well-stacked discs in the outer segments (indicated by *white arrows* in Fig. 2*C*). In contrast, the cone outer segments in *exoc5* mutants were significantly fewer in number, shorter in length, and disorganized (Fig. 2*D*). Such abnormalities were never observed in retinal sections of WT siblings. Taken together, these results indicate that eye development, proper retinal lamination, and outer segment morphogenesis requires *exoc5* function.

Loss of exoc5 results in shorter photoreceptor outer segment length and loss of cilia in zebrafish

We next used immunohistochemistry to determine whether localization and trafficking of photoreceptor outer segment proteins occurred normally in *exoc5* mutants. At 3.5 dpf, rhodopsin localized normally to the rod outer segments of WT fish (Fig. 3*A*). In *exoc5* mutants, rudimentary outer segment localization of rhodopsin was observed, together with some rhodop-

sin being mislocalized to the inner segments (Fig. 3*B*). To quantify the lengths of the outer segments, we used rhodopsin immunoreactivity as a surrogate, determining the extent of rhodopsin staining along the proximal–distal axis of the outer segments. In WT siblings, outer segments were 7.9 ± 0.45 μm in length (n = 20 embryos, 130 outer segments), whereas *exoc5* mutant outer segment were 3.2 ± 0.23 μm in length (60.5% shorter, $p < 0.001$; n = 12 embryos, 60 outer segments) (Fig. 3*G*). To determine whether these shortened outer segments correlated with cilia formation, we labeled retina sections with antibodies against acetylated α-tubulin, a marker that is required and sufficient to determine the presence of photoreceptor cilia (30). Although retina sections in WT zebrafish showed the presence of cilia, we could not detect cilia in the retina sections of *exoc5* mutants (Fig. 3, *C* and *D*). We next examined cone morphology, the predominant photoreceptor cell type in the zebrafish retina, by immunolabeling with peanut agglutinin lectin (PNA-488), which labels the interphotoreceptor matrix surrounding cone outer segments and, to some extent, the retinal plexiform layers (31). Peanut agglutinin lectin staining revealed that the *exoc5* mutant cone outer segments were significantly shorter (5.8 ± 0.33 μm in WT *versus* 2.2 ± 0.24 μm in mutants; $p < 0.001$), disorganized, and misshapen (Fig. 3, *E*, *F*, and *H*). Additionally, the number of cone outer segments was significantly fewer in number in *exoc5* mutants compared with WT siblings (Fig. 3, *E* and *F*), which suggested that loss of *exoc5* results in defective cone outer segment morphogenesis. These data demonstrate that *exoc5* is indispensable for cilia and subsequent photoreceptor outer segment formation in zebrafish.

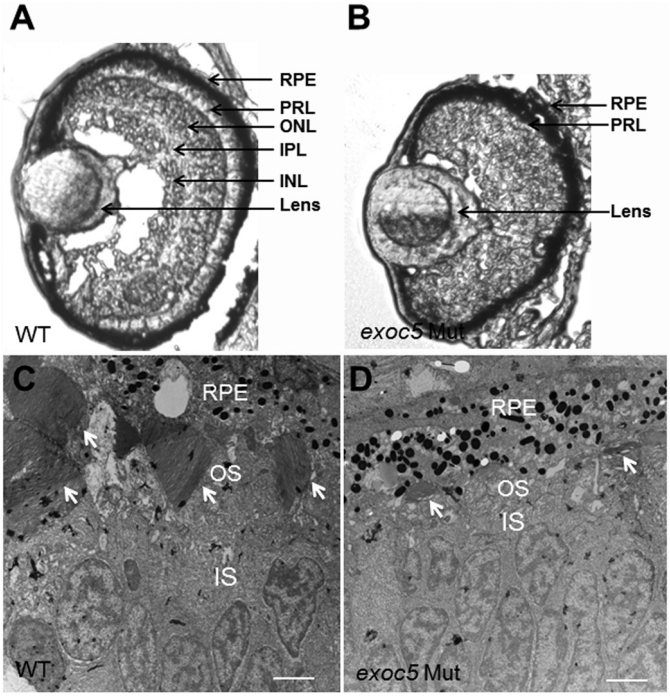

Figure 2. Histologic analysis of retinas of wild-type and *exoc5* mutant zebrafish larvae. *A* and *B*, transverse sections of 3.5-dpf WT (*A*) and exoc5 mutant (*B, exoc5 Mut*) eyes. In *exoc5* homozygous mutants, retinal lamination was lost, and the photoreceptor outer segments (*arrows*; photoreceptor layer (*PRL*)) were disorganized and not readily detectable. *C* and *D*, ultrastructural analysis of WT and *exoc5* mutant photoreceptors using transmission electron microscopy. *C*, WT photoreceptors showed tightly stacked disc membranes (*arrows*) and inner segments; *D*, in *exoc5* mutants only remnants of outer segments (*arrows*) could be observed. *Scale bars*, 2 μm (*C* and *D*). *OS*, outer segments; *IS*, inner segments; *ONL*, outer nuclear layer; *RPE*, retinal pigmented epithelium.

Conditional Exoc5 knock-out mice show defects in photoreceptor development

Photoreceptor-specific knockout of *Exoc5* in mice was accomplished by crossing the *Exoc5* fl/fl mouse line, which we made using embryonic stem (ES) cells from the European conditional mouse mutagenesis (EUCOMM) consortium (clone

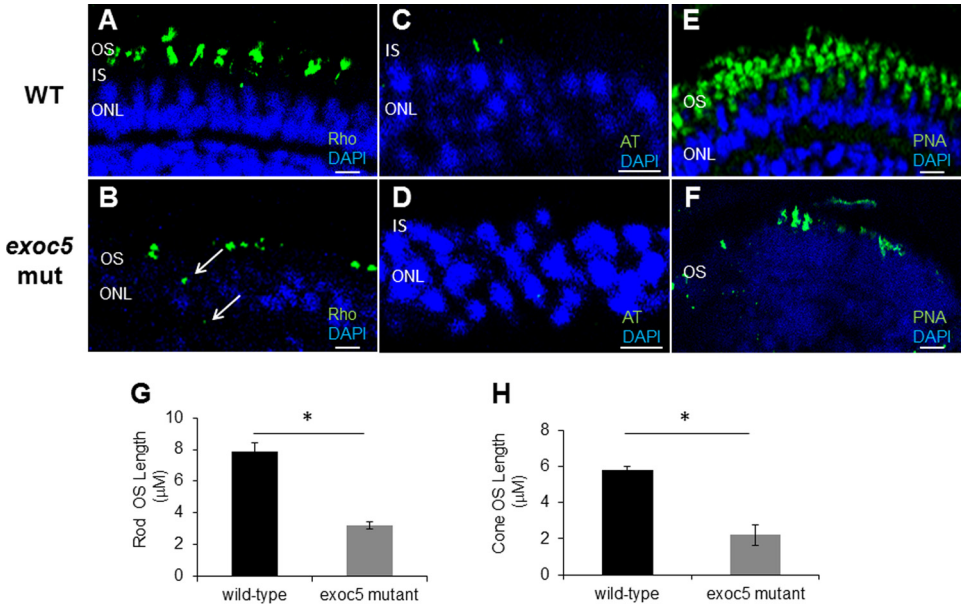

Figure 3. Immunohistochemical analysis of rod and cone photoreceptors in wild-type and *exoc5* mutant zebrafish. Rod photoreceptor outer segments were identified with 1D4 antibody specific for rhodopsin (*green*, *Rho*, *A* and *B*); cilia with α-acetylated tubulin (*green*, *AT*, *C* and *D*); and cone photoreceptors with PNA-lectin-488 (*green*, PNA, *E* and *F*), all at 3.5 dpf. *Arrows* in *B* highlight rhodopsin mislocalization in *exoc5* mutants. Severe loss of rod and cone pigment proteins as well as a lack of cilia was noted in the mutant zebrafish. Quantification of photoreceptor outer segment length at 3.5 dpf is provided for rods (*G*) and cones (*H*). *, $p < 0.05$. *Scale bars*, 25 μm (*A, B, E,* and *F*) and 10 μm (*C* and *D*). *OS*, outer segments; *IS*, inner segments; *ONL*, outer nuclear layer.

number DEPD00521_3) (32), with a rhodopsin-Cre driver line. The conditional target mouse line, designated as *Exoc5*fl/fl; Rho-Cre$^+$, was confirmed by PCR-based genotyping (supplemental Fig. 2). Histologic analyses in frozen sections of retinas from WT and *Exoc5* fl/fl;Rho-Cre$^+$ mice revealed severe thinning of the outer retina in postnatal day 30 (P30) mice (Fig. 4*B*), when compared with WT animals (Fig. 4*A*). Disorganization and lack of photoreceptor outer segments were more obvious by transmission electron microscopy of conditional *Exoc5* knock-out animals. In WT siblings at P30, photoreceptor outer segments extended toward the RPE in a parallel and organized manner, giving a palisade pattern (Fig. 5, *A* and *C*). In contrast, the photoreceptor outer segments in *Exoc5* fl/fl;Rho-Cre$^+$ mice were significantly fewer in number, shorter in length, and disorganized (Fig. 5, *B* and *D*). We further examined the structure of the photoreceptor sensory cilium components in WT and *Exoc5* fl/fl;Rho-Cre$^+$ retinas. The stacks of nascent discs were organized and were oriented perpendicular to the long axis of the axoneme that extended from the basal body and transition zone in WT mice (Fig. 5*E*). In contrast, we did not observe connecting cilia components in *Exoc5* fl/fl;Rho-Cre$^+$ retinas (Fig. 5*F*). Taken together, these results indicate that outer segment morphogenesis requires Exoc5 function, and Exoc5 is necessary for photoreceptor ciliogenesis in mice.

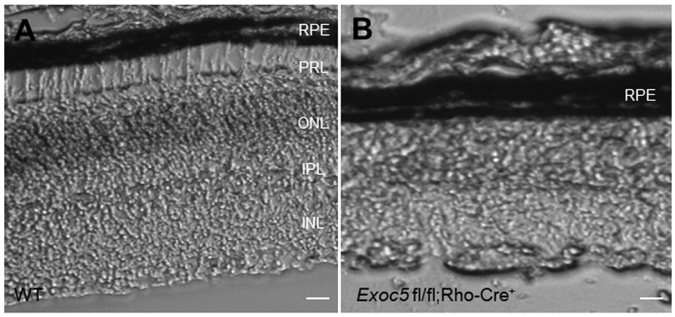

Figure 4. Histologic analysis of retinas of P30 *Exoc5* conditional mice. *A* and *B,* transverse retina cryosections of WT (*A*) and photoreceptor-specific *Exoc5* knock-out (*Exoc5* fl/fl; Rho-Cre$^+$) (*B*) mice revealed a thinning of the outer retina in P30 *Exoc5* conditional photoreceptor knock-out mice. *Scale bars,* 125 μm (*A* and *B*). *RPE,* retinal pigmented epithelium; *OS,* outer segments; *IS,* inner segments; *ONL,* outer nuclear layer; *IPL,* inner plexiform layer; *INL,* inner nuclear layer; *PRL,* photoreceptor layer.

Altered photoreceptor outer segment protein targeting and levels in Exoc5 fl/fl;Rho-Cre+ mice

In WT mice, rhodopsin was localized specifically to the outer segments by P30 (Fig. 6*A*). In contrast, *Exoc5* fl/fl;Rho-Cre$^+$ mouse retinas exhibited significantly decreased levels of rhodopsin, and the rhodopsin was not specifically localized to the outer segments (Fig. 6*B*). Indeed, in *Exoc5* fl/flRho-Cre$^+$ mice, rhodopsin was aberrantly distributed to the inner portion of the ONL (cell bodies), as well to the inner segments of photoreceptors, indicating a defect in cilia trafficking (Fig. 6*B*). As we did for zebrafish retinas, rhodopsin immunoreactivity along the axis of the outer segment was used to document a shortened outer segment length in mutant mice (Fig. 6*G*). Photoreceptor degeneration, as indicated by a thinning of the ONL, was observed in retinas from *Exoc5* fl/fl;Rho-Cre$^+$ mice by P30, a time at which the ONL was only ~2–3 cells thick (Fig. 6, *A*–*F*). To determine whether this ONL cell loss correlated with an absence of cilia, we labeled retinal sections with antibodies against acetylated α-tubulin. Although many cilia were detected in retinal sections in WT animals throughout the ONL, no cilia were seen in the retinal sections of *Exoc5* fl/fl;

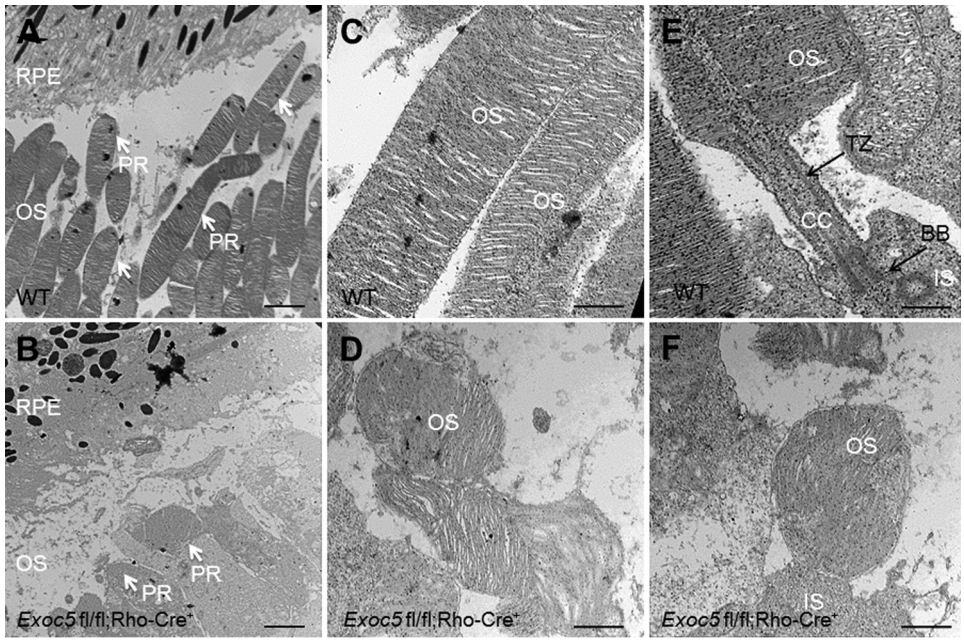

Figure 5. Ultrastructural analysis of wild-type and conditional *Exoc5* knock-out mouse photoreceptors. Transmission electron microscopy provided ultrastructural views of wild-type (*WT*) and *Exoc5* fl/fl;Rho-Cre$^+$ mice photoreceptor cells. *A* and *C,* WT rod photoreceptors (*PR*) showed tightly stacked disc membranes (*arrows*); *B* and *D,* rod outer segments of *Exoc5* fl/fl;Rho-Cre$^+$ mouse retinas contained fewer disks and lacked proper stacking. *E* and *F,* details of the photoreceptor sensory cilium components, in retinas from P30 WT (*E*) and *Exoc5* fl/fl;Rho-Cre$^+$ (*F*) mice. The stacks of nascent discs, the axoneme, basal body, and transition zone had a normal appearance in WT mice, but no ciliary components were detected in the *Exoc5* fl/fl;Rho-Cre$^+$ mice. *Scale bars,* 800 nm (*A* and *B*); 400 nm (*C* and *D*); 100 nm (*E* and *F*). *RPE,* retinal pigmented epithelium; *OS,* outer segments; *IS,* inner segments; *CC,* connecting cilium; *TZ,* transition zone; *BB,* basal body; *PR,* photoreceptor.

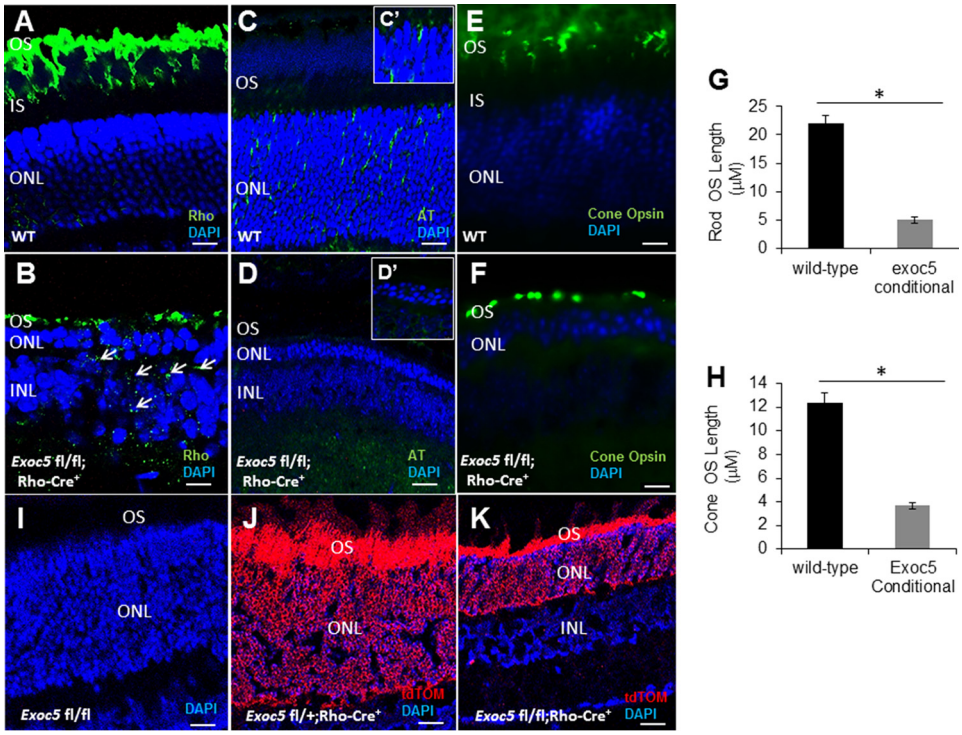

Figure 6. Immunohistochemical analysis of rod and cone photoreceptors in wild-type and conditional *Exoc5* knock-out mice. *A* and *B,* levels and localization of rhodopsin (*green*, Rho); *C* and *D,* α-acetylated tubulin (*green,* AT); and *E* and *F, red/green* cone opsins (*green,* cone opsin) were used at P30 to identify alterations in cilia and in rod and cone outer segments. *Arrows* in *B* highlight rhodopsin mislocalization in *Exoc5* conditional knock-out mouse retinas. Rod (*G*) and cone (*H*) outer segment lengths were quantified based on the thickness of the respective outer segment areas. *I–K,* Ai14 Cre reporter mice that harbor a loxP-flanked STOP cassette preventing transcription of a CAG promoter-driven red fluorescent protein variant (tdTomato) were mated to *Exoc5fl/fl* mice, so that tdTomato expression in a cell indicates Exoc5 has been inactivated by Cre. No tdTomato expression was seen in *tdTomato Exoc5fl/fl* mice (*I*), although tdTomato expression was seen in heterozygous *tdTomato Exoc5fl/+;Rho-Cre/+* mice, which had normal photoreceptor and outer segment histology (*J*), and tdTomato expression was also seen in homozygous *tdTomato Exoc5fl/fl;Rho-Cre/+* mice, which had markedly abnormal photoreceptor histology and minimal outer segment formation (*K*). *Scale bars,* 25 μm (*A, B, E,* and *F*), 50 μm (*C* and *D*), and 100 μm (*I–K*). *, $p < 0.05$. *OS,* outer segments; *IS,* inner segments; *ONL,* outer nuclear layer; *INL,* inner nuclear layer.

Rho-Cre$^+$ mice at P30 (Fig. 6, *C* and *D*). Cone morphology was examined by immunolabeling with anti-red/green cone opsin antibody. Cone opsin staining revealed the presence of long and well-organized cone outer segments in WT mice, whereas *Exoc5* fl/fl;Rho-Cre$^+$ mouse cone outer segments were significantly shorter and appeared disorganized and misshapen (Fig. 6, *E*, *F,* and quantified in *H*). These results demonstrate that *Exoc5* is crucial for cilia and rod photoreceptor outer segment formation in mice. Effects on the survival of cones in the *Exoc5* fl/fl;Rho-Cre/+ mice are predicted to be due to the known survival effect of rods on cones (33). To confirm the photoreceptor-specific knockout, Ai14 Cre reporter mice that harbor a loxP-flanked STOP cassette preventing transcription of a CAG promoter-driven red fluorescent protein variant (tdTomato), congenic on the C57BL/6J genetic background, were then mated to *Exoc5fl/fl* mice, so the tdTomato expression in a cell indicates Exoc5 has been inactivated by Cre. No tdTomato expression was seen in *tdTomato Exoc5fl/fl* mice (Fig. 6*I*), whereas tdTomato expression was seen in heterozygous *tdTomato Exoc5fl/+;Rho-Cre/+* mice, which had normal photoreceptor and outer segment histology (Fig. 6*J*), and tdTomato expression was also seen in homozygous *tdTomato Exoc5fl/fl;Rho-Cre/+* mice, which had markedly abnormal photoreceptor histology and minimal outer segment formation (Fig. 6*K*).

Exoc5 fl/fl;Rho-Cre$^+$ mice show significantly reduced visual function by electroretinography (ERG)

To correlate retinal structure with function, ERG responses were analyzed under dark-adapted scotopic conditions to determine rod photoreceptor function (Fig. 7, *A* and *B*), as well as under photopic conditions after light adaptation to determine cone function (Fig. 7*C*) in Exoc5 fl/fl, Exoc5 fl/+, *Exoc5* fl/+;Rho-Cre$^+$ (control), and *Exoc5* fl/fl;Rho-Cre+ (photoreceptor-conditional knock-out mutant) mice. At 30 days of age, both rod a- and b-wave amplitudes were significantly reduced (~50–60%) across the spectrum of light intensities recorded (Fig. 7, *A* and *B*). A repeated measure ANOVA revealed an amplitude by genotype interaction (a-waves, $p < 0.0001$; b-waves, $p < 0.0001$). A post hoc ANOVA determined that this difference was driven entirely by the *Exoc5* fl/fl;Rho-Cre$^+$ mice; the three control groups had a- and b-wave amplitudes that were indistinguishable from each other (a-waves, $p > 0.4$; b-waves, $p > 0.2$), whereas the three control groups individually (a-waves, $p < 0.03$ to $p < 0.006$; b-waves, $p < 0.01$ to $p < 0.002$), or combined (a-waves, $p < 0.0005$; b-waves, $p < 0.001$), were significantly different from the *Exoc5* fl/fl;Rho-Cre$^+$ mice. In contrast, there was no statistical difference in the cone amplitudes between the four groups at P30 ((in μV) Exoc5 fl/fl, 152 ± 5.1; Exoc5 fl/+, 197 ± 13.0; *Exoc5* fl/+;Rho-Cre$^+$, 177 ± 14.0; and *Exoc5* fl/fl;Rho-Cre$^+$, 143 ± 12.8; mean ± S.E., $p > 0.06$).

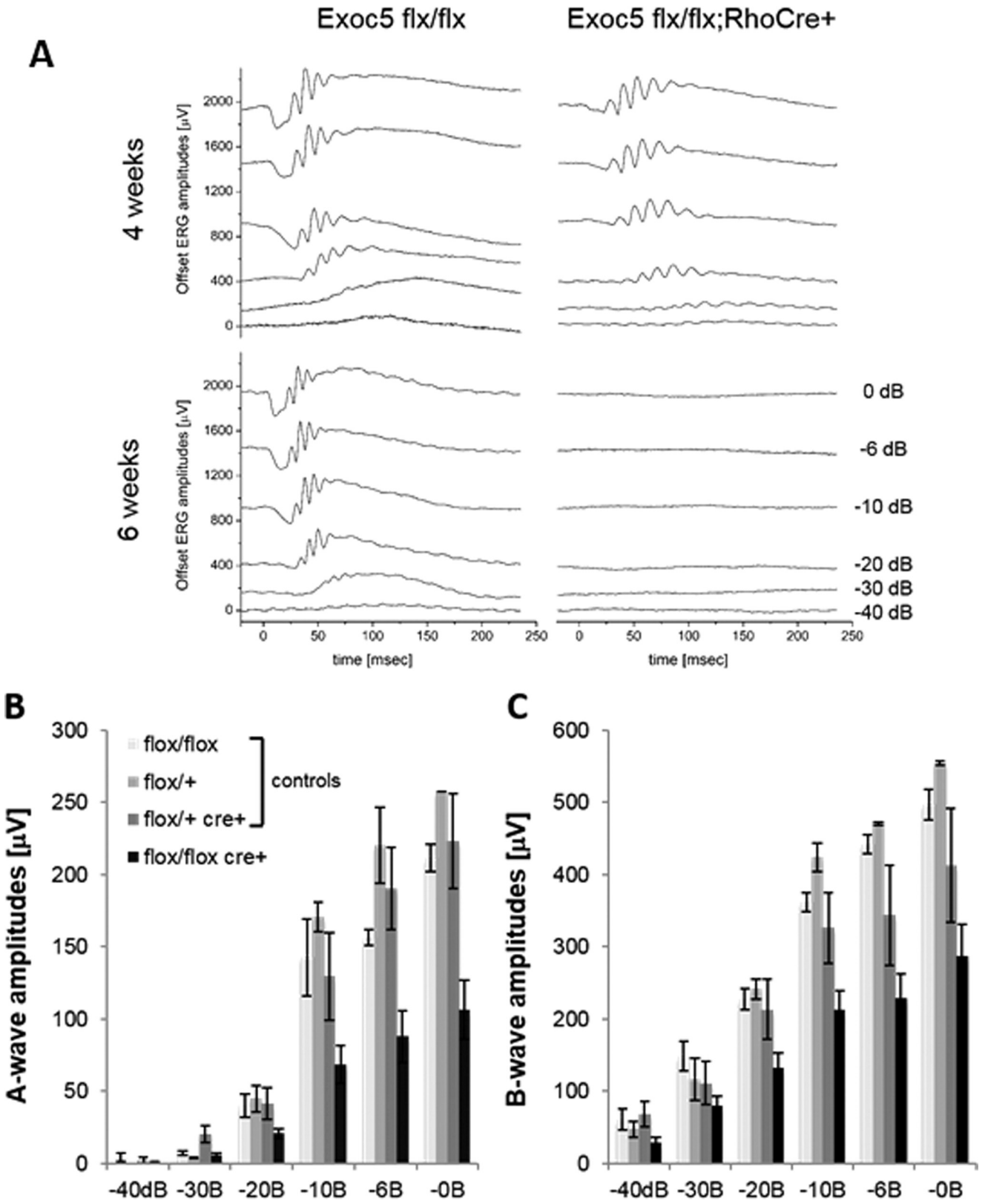

Figure 7. Measurement of visual function by full-field ERG. Dark-adapted scotopic ERGs were recorded in response to increasing light intensities in cohorts of 30-day-old control (*Exoc5* fl/fl, *Exoc5* fl/$^{+}$, and *Exoc5* fl/$^{+}$;Rho-Cre^{+}) and *Exoc5* fl/fl;Rho-Cre^{+} mice. *A–C,* photoreceptor-specific knock-out mice in which both copies of Exoc5 were eliminated had significantly lower dark-adapted a- and b-wave amplitudes compared with controls (post hoc ANOVA: a-waves, $p < 0.03$; b-waves, $p < 0.01$), in particular at higher light intensities (20, 10, 6, 0 db). Photoreceptor cell responses (a-waves), which drive the b-waves, were equally affected (both reduced on average between 50 and 60%). Data are expressed as mean ± S.E. (Exoc5 fl/fl, $n = 3$; Exoc5 fl/+, $n = 2$; Exoc5 fl/+;Rho-Cre^{+}, $n = 5$; and *Exoc5* fl/fl;Rho-Cre^{+} mice, $n = 10$).

All visually evoked responses for both rods and cones, however, were completely eliminated in the *Exoc5* fl/fl;Rho-Cre$^+$ by 42 days, and there was no significant difference in rod a- or b-waves or cones in a control group at 30 or 42 days (Exoc5 fl/fl; a-waves, $p = 0.88$; b-waves, $p = 0.32$; cones, $p = 0.64$).

Discussion

We report two principal findings here, both of which are of great interest. First, we show that the exocyst, which is required for ciliogenesis in the kidney, is also necessary for ciliogenesis in the eye. Second, we report that the strikingly severe phenotype following knockout of Exoc5 translates across species, from zebrafish to mammals.

We had previously shown in MDCK cells that shRNA-mediated knockdown of Exoc5 inhibited ciliogenesis, led to increased cell proliferation, and resulted in low intracellular calcium levels that did not increase in response to fluid flow, all features consistent with polycystic kidney disease (PKD). *Exoc5* overexpression in MDCK cells, however, resulted in longer cilia, with normal intracellular calcium levels and an enhanced response to fluid flow. Cell polarity was not grossly affected (21, 23). These data demonstrated a critical role for the exocyst in renal ciliogenesis; however, the question of whether this pathway was conserved across different organs and species had never been tested in suitable animal models.

The exocyst is thought to function as a holocomplex that targets and docks vesicles carrying membrane-bound proteins from the trans-Golgi network (34). PKD2, which encodes polycystin-2, is one of two genes that, when mutated, leads to autosomal dominant polycystic kidney disease, the most common ciliopathy, and the most common potentially lethal genetic disease to affect humans (6). We have shown in the kidney that a major role of the exocyst is to traffic vesicles carrying ciliary proteins, such as polycystin-2, to the nascent primary cilium (21–24, 35). For example, polycystin-2 biochemically interacts with Exoc5 protein, co-localizes with the exocyst at the primary cilium in wild-type cells, and is mislocalized intracellularly following knockdown of Exoc5 (23). Of note, many zebrafish cilia mutants are known to have a curly tail down phenotype; however, to our knowledge, the only other mutants with a curly tail up phenotype similar to our *exoc5* mutants are the *pkd* mutants (23).

It is well known that ciliary proteins are conserved across organs and species, but it has been an open question regarding the conservation of trafficking pathways needed to generate primary cilia. Indeed, in RPE cells, Nachury *et al.* (20) had identified ciliary Bardet-Biedl proteins, which together form the "BBsome," as being centrally involved in vesicular transport *to* the primary cilium (20), although later work suggests that the BBsome is actually involved in exporting proteins *from* the cilium (36). The fact that we show here that the exocyst regulates ciliogenesis in the zebrafish and mouse eye, as well as the kidney, indicates that at least some primary ciliogenic trafficking programs are conserved across species and organs. This also helps to explain why exocyst mutations in families can lead to both kidney and eye phenotypes. Joubert and Meckel's syndromes are ciliopathies that affect multiple organs, including the eye and kidney, and human families have recently been identified with exocyst mutations (37, 38). Interestingly, mutations in the exocyst have also been shown to lead to optic nerve aplasia, which can result in retinal dysplasia (39). Importantly, in three reports of human mutations of exocyst complex members, mutations in one allele were enough to result in disease (39–41). This dominant mode of expression could be a result of the mutation leading to gain-of-function, dominant-negative expression, haploinsufficiency, or loss-of-heterozygosity. It may also explain why more exocyst ciliopathies have not been found, as most ciliopathies, such as nephronophthisis, Bardet-Biedl, and ARPKD, are recessive in nature, and single allele mutations would not have been flagged.

The second important finding is the observation of a similar severe and striking retinal phenotype in both zebrafish and mice following knockout of *Exoc5*. Although it is formally possible that that the effect of Exoc5 loss in other tissues, such as the RPE, could influence the photoreceptor phenotype, we think that this is highly unlikely given the lack of tdTomato expression in tissue other than the photoreceptor cells in *tdTomato Exoc5fl/+;Rho-Cre/+* mice. Additionally, although tdTomato expression was seen in heterozygous *tdTomato Exoc5fl/+;Rho-Cre/+* mice, the phenotype was normal photoreceptor and outer segment histology (Fig. 6*J*). tdTomato expression was also seen in homozygous *tdTomato Exoc5fl/fl; Rho-Cre/+* mice, which had markedly abnormal photoreceptor histology and minimal outer segment formation. Thus, the genotype/phenotype expression was highly correlated. The development and maintenance of photoreceptor cells is known to be heavily dependent on functional ciliary intracellular trafficking. A major strength of this study is that we used two different animal models, zebrafish and mouse, each of which has specific advantages that can be exploited to investigate the role of the exocyst in photoreceptor and eye development. The data in zebrafish and mice presented here demonstrate that Exoc5 is required for photoreceptor outer segment development and that the deficiency of Exoc5 results in a lack of photoreceptor ciliogenesis and outer segment protein mis-localization, leading to photoreceptor cell loss and blindness by 6 weeks of age in mice. In zebrafish, we took advantage of the ability to easily rescue *exoc5* mutants by injection of one- to two-cell stage embryos with human EXOC5 mRNA, confirming that the *exoc5* mutant phenotype was specifically due to lack of functional *exoc5*. We were also able to show activation of the Hippo pathway in *exoc5* mutants. We and others have linked the Hippo pathway to cilia and PKD (29, 42), and activation of the Hippo pathway has also been shown to control organ size (28, 29). Activation of the Hippo pathway could help explain the small eye phenotype that we saw in *exoc5* mutant zebrafish. This would be an area ripe for therapeutic investigation, as there are many small-molecule modulators of the Hippo pathway, some of which have already been approved by the Food and Drug Administration (43). The failure of outer segment development in *exoc5* mutant zebrafish and conditional *Exoc5* knock-out mice is almost complete and is likely due to a ciliary trafficking defect, as evidenced by mis-localization of outer segment protein to the inner segments, along with a lack of cilia formation. The effects of the rod-specific loss of Exoc5 on cone outer segment development are predicted to be due to the

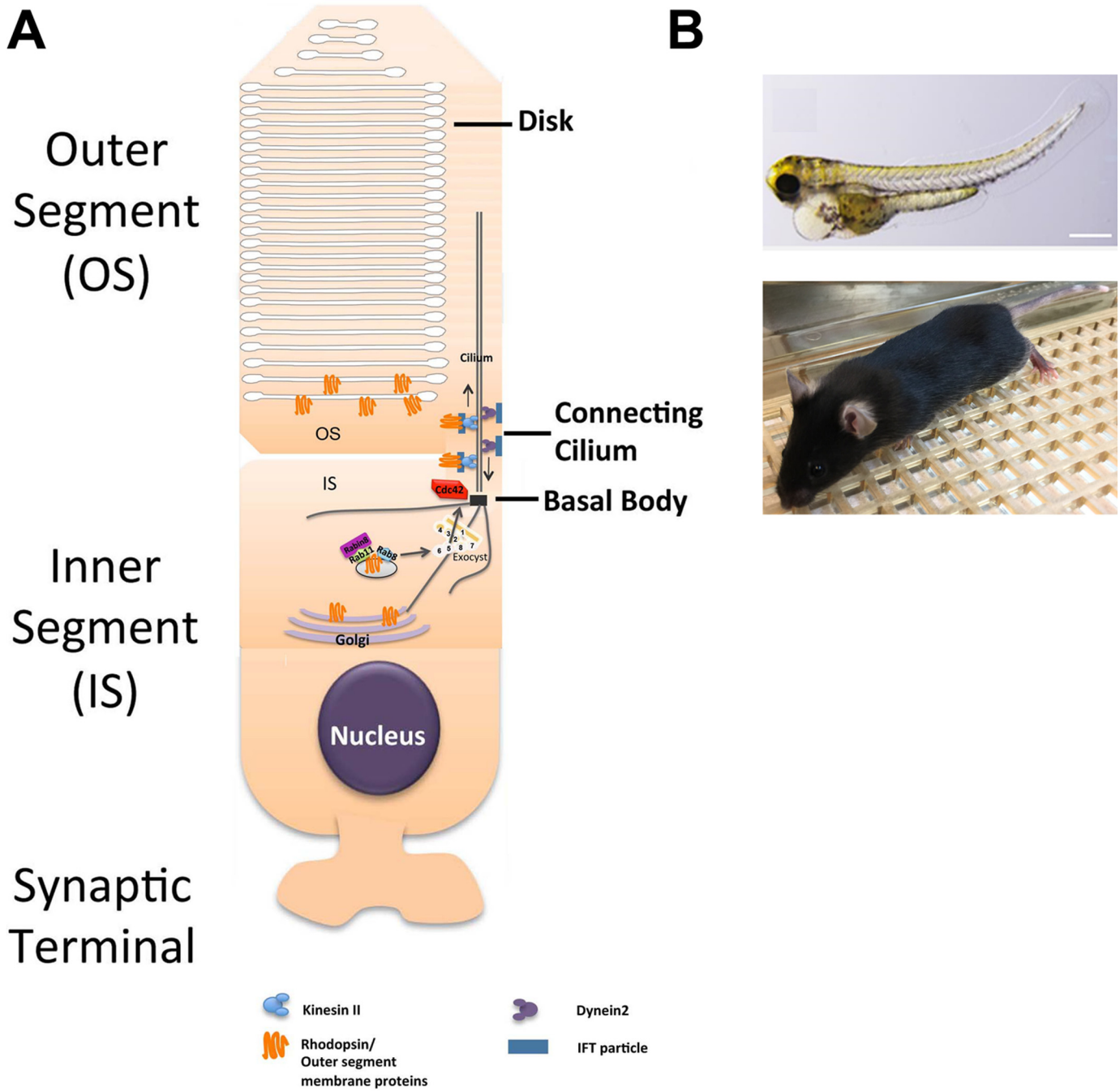

Figure 8. Model for exocyst-mediated trafficking of ciliary and outer segment proteins. *A,* mRNA is generated by transcription in the nucleus, and proteins are translated from mRNA in the endoplasmic reticulum and then sent to the trans-Golgi network for packaging into vesicles for transport to their final cellular destination. Ciliary and outer segment proteins are found in vesicles that have a small GTPase, Rab8, on the surface, which binds to exocyst complex member Exoc6. Exoc6, bound to the vesicle containing the ciliary and outer segment proteins, then interacts with the central exocyst complex protein Exoc5, which, in turn, brings the vesicle to the rest of the exocyst, itself localized to the primary cilium by another small GTPase, Cdc42. *B,* when this ciliogenic pathway is perturbed, the result in a global zebrafish knockout of *exoc5* is defects in multiple ciliated organs, including the eye. In mice with a photoreceptor-specific knockout of Exoc5, the result is retinal degeneration and blindness. *Scale bar,* 0.268 mm.

known survival effect of rods on cones (33) (*e.g.* PNA lectin localization from collapsed cone outer segments to the OPL and IPL has been observed in retina degeneration models (44)). Given the histologic severity of the phenotype, it is not surprising that, by ERG testing, the *Exoc5* photoreceptor-specific knock-out mice were completely blind by 6 weeks of age.

In summary, we show here that exocyst-mediated ciliogenesis programs are conserved in both the kidney and eye and in both zebrafish and mice. We also show that the exocyst is essential for photoreceptor outer segment development and maintenance, most likely by trafficking ciliary proteins from the inner segments to the outer segment (Fig. 8). The zebrafish and mouse *Exoc5* knockouts described here could also be useful as animal models of retinal degeneration, upon which therapeutic compounds could then be tested.

Experimental procedures

Materials

All chemicals, unless stated otherwise, were purchased from Sigma.

Animal approval

All experiments on zebrafish and mice were approved by the Institutional Animal Care and Use Committee (IACUC) of the Medical University of South Carolina, and they were performed in compliance with the ARVO Statement for the Use of Animals in Ophthalmic and Vision Research.

Zebrafish husbandry

Adult zebrafish were maintained and raised in an Aquatic Habitats recirculating water system (Tecniplast, West Chester, PA) in a 14:10-h light/dark cycle. The *exoc5* mutant zebrafish line was purchased from the Zebrafish International Resource Center (ZIRC, Eugene, OR: *exoc5*-sa23168). This *exoc5* zebrafish mutant, contains a Cys → Thr point mutation at amino acid 377, resulting in a premature stop codon. The point mutation was verified by PCR and direct sequencing of both strands in both heterozygote adults and mutant larvae progeny. Genomic DNA from clipped fins, or whole 3.5 dpf zebrafish with phenotypes, was extracted in 50 μl of 1× lysis buffer (10 mM Tris-HCl, pH 8.0, 50 mM KCl, 0.3% Tween 20, 0.3% Nonidet P-40), denatured at 98 °C for 10 min, and digested at 55 °C for 6 h after 10 μg/ml proteinase K was added, and the reaction was stopped at 98 °C for 10 min. The PCR primers used were as follows: forward primer, 5′-CTATATAGACATGGAGCGGCAAT-3′; reverse primer, 5′-CCAACAATTCCTCACCTTCC-3′. Sequencing was performed by Genewiz with the forward primer used for PCR (Genewiz, South Plainfield, NJ). The second mutant *exoc5* zebrafish line was generated by Dr. John Parant in Core B of the UAB P30 Hepatorenal Fibrocystic Disease Core Center using CRISPR gene editing. The CRISPR mutation was identified as a 13-bp insertion in exon 4, leading to a frameshift and premature stop codon. To confirm the mutation, genomic DNA from clipped fins, or whole 3 dpf zebrafish with phenotypes, was extracted in 50 μl of 1× lysis buffer (10 mM Tris-HCl, pH 8.0, 50 mM KCl, 0.3% Tween 20, 0.3% Nonidet P-40), denatured at 98 °C for 10 min, digested at 55 °C for 6 h after 4 μl of 10 mg/ml proteinase K was added, and the reaction was stopped at 98 °C for 10 min. The PCR primers used were as follows: forward primer, 5′-CAAAGGTAGCCTTCCAGCAC-3′; reverse primer: 5′-CCTCTGTCTCGGGGTATTGA-3′. Sequencing was performed by Eurofins with the forward primer, 5′-TCCAGCATGTTTTTCTGGTG-3′.

Mouse husbandry

Animals were kept in a 12-h light/dark cycle with food and water *ad libitum*. The generation and genotyping of our *Exoc5* (also known as Sec10) fl/fl mice has been described previously (32). The photoreceptor-specific conditional *Exoc5* knock-out mice were generated by crossing *Exoc5* fl/fl with rhodopsin-Cre$^+$ mice (The Jackson Laboratory, Bar Harbor, ME) and are designated as *Exoc5* fl/fl;Rho-Cre$^+$ in this study. *Exoc5* conditional mice were genotyped using the following set of PCR primers: forward primer, Fl-Exoc5 5′loxP#2F 5′-GCCTGTAACTCACAGAGATC-3′; reverse primer, Fl-Exoc5 5′loxP#2R 5′-GCTGGCATTCTAAGTCATGG-3′. Rho-Cre mice were identified using the following set of PCR primers: forward primer, 5′-TCAGTGCCTGGAGTTGCGCTGTGG; reverse primer: 5′-TTCAAAGGCCAGGGCCTGCTTGGC. To confirm the specificity of the *Exoc5* knockout, Ai14 Cre reporter mice that harbor a loxP-flanked STOP cassette preventing transcription of a CAG promoter-driven red fluorescent protein variant (tdTomato), congenic on the C57BL/6J genetic background, were then mated to *Exoc5fl/fl* mice, so that tdTomato (red) expression in a cell indicates *Exoc5* has been inactivated by Cre.

Mouse retina dissection, immunohistochemistry, and fluorescence imaging

P30 mouse eyes were enucleated and fixed by immersion in 4% paraformaldehyde in 1× phosphate buffer (PBS) for 2 h at room temperature. Eyes were incubated in a sucrose gradient of 5% sucrose in phosphate buffer (SPB) for 15 min at room temperature, 15% SPB for 15 min at room temperature, 30% SPB for 1 h at room temperature, and overnight in a 70:30 v/v ratio of OCT/SPB solution (Tissue-Tek, Sakura Finetech, Torrance, CA) at 4 °C. Eyes were then mounted in cyro-molds containing 70:30 v/v ratio of OCT/SPB solution and frozen on a dry-ice bath containing 100% ethanol. 12-μm-thick sections were cut using a cryostat (Leica). Sections were air-dried for 24 h at room temperature and then subjected to immunohistochemistry. Blocking solution (1% BSA, 5% normal goat serum, 0.2% Triton X-100, 0.1% Tween 20 in PBS) was applied for 2 h in a humidified chamber. Primary antibodies were diluted in blocking solution as follows: 1D4 (1:100, Abcam, Cambridge, MA) and acetylated α-tubulin (1:1000; Sigma). Cones were stained with Alexa Fluor 488-conjugated peanut lectins (PNA-488, at 1:250, Molecular Probes, Eugene, OR). Conjugated secondary antibodies were purchased from Invitrogen Life Technologies, Inc., and used at 1:500 dilutions, and 4′,6-diamidino-2-phenylindole (DAPI; 1:1000) was used to label nuclei. Sections were mounted in Vectashield (Vector Laboratories, Burlingame, CA). Z-stack images were collected using a Leica SP8 confocal microscope (Leica, Germany) and processed with the Leica Viewer software.

Zebrafish immunohistochemistry and fluorescence imaging

3.5 dpf larvae were fixed using different protocols, depending on the primary antibodies being used. For ID4, lectin peanut agglutinin-conjugated Alexa Fluor 488 (PNA-488), Red/Green cone opsins, and acetylated tubulin samples were fixed in 4% paraformaldehyde in 1× PBS at 4 °C overnight. All samples were cryoprotected in 30% sucrose for 48 h. Cryosections (10 μm) were cut and dried on frost-free slides at room temperature overnight. Blocking solution (1% BSA, 5% normal goat serum, 0.2% Triton X-100, 0.1% Tween 20 in 1× PBS) was applied for 2 h in a humidified chamber. Primary antibodies and lectins were diluted in blocking solution as follows: 1D4 (1:100, Abcam, Cambridge, MA), PNA-488 (1:1000, Molecular Probes, Eugene, OR), Red/Green cone opsin (1:1000, MilliporeSigma,

Billerica, MA), and acetylated-α-tubulin (1:5000; Sigma). Conjugated secondary antibodies were purchased from Invitrogen Life Technologies, Inc., and used at 1:500 dilutions, and DAPI at 1:1000 was used to label nuclei. For whole-mount analysis of the kidney cilia, 36-hpf embryos were fixed in Dent's fixative (80% methanol, 20% dimethyl sulfoxide (DMSO)) overnight at room temperature. The next day, whole-mount immunostaining was performed as follows: embryos were rehydrated in a graded series of methanol, buffered in 1× PBST (MeOH/PBST), washed for 15 min each at room temperature, and incubated in blocking solution (PBS, 1% DMSO, 0.5% Tween 20, 1% BSA, 10% normal goat serum) overnight at 4 °C. Embryos were incubated with a mouse anti-acetylated α-tubulin primary antibody (1:500) diluted in incubation solution (PBS, 1% DMSO, 0.5% Tween 20, 2% normal goat serum) for a minimum of 36 h at 4 °C. Embryos then were washed four times with incubation solution for 30 min each and incubated with a fluorophore-conjugated secondary antibody (1:1000) diluted in incubation solution overnight at 4 °C. Following antibody staining, embryos were washed again with incubation solution and mounted on slides for imaging. Optical sections were obtained with a Leica SP8 confocal microscope (Leica, Germany) and processed with the Leica Viewer software.

Western blot analysis

Dechorionated zebrafish embryos at 3.5 or 4 dpf were homogenized in SDS sample buffer containing protease inhibitor mixture (Sigma) and phosphatase inhibitor (Thermo Fisher Scientific, Rockford, IL) to perform Western blot analysis. The homogenized lysates were boiled for 5 min at 95 °C followed by centrifugation at 13,500 rpm for 20 min at 4 °C, and the supernatants were collected and mixed with 3× Laemmli sample buffer for the protein electrophoresis. The protein samples were separated on NuPAGE 4–12% BisTris gels (Novex, Carlsbad, CA) and then transferred to a nitrocellulose membrane (Novex, Carlsbad, CA). The antibodies used in this study are as follows: rabbit polyclonal anti-Exoc5, which was described previously (21); mouse anti-Exoc4 (Enzo, Farmingdale, NY); rabbit anti-MOB1 and phospho-MOB1 (Thr-35) (Cell Signaling Technology, Inc.); and mouse anti-GAPDH monoclonal antibody (Sigma), all at 1:1000 dilution. Secondary antibodies were from Jackson ImmunoResearch and Thermo Fisher Scientific.

Exoc5 mutant mRNA rescue experiments

For rescue experiments of zebrafish *exoc5* mutants, capped and polyadenylated mRNA of wild-type (WT) human *EXOC5* was synthesized *in vitro* using the message machine kit (Ambion, Austin, TX). Two doses of WT *EXOC5* mRNA (low, 100 pg or high, 250 pg) were injected, using a Sutter Instruments Microinject, into 100 embryos, at the one- to two-cell development stage. At 3.5 dpf, 12 randomly selected injected larvae were imaged and then individually genotyped by direct sequencing as outlined above.

Transmission electron microscopy

Control and *exoc5* mutant larvae or WT and *Exoc5* fl/fl;Rho-Cre^{+} mouse eyes (or eyecups) were fixed in a solution containing 2.5% glutaraldehyde, 2% paraformaldehyde, and postfixed with 2% osmium tetroxide. The fixed tissue was sectioned to obtain radial sections at 1 μm and rinsed with cacodylate buffer (0.1 M), dehydrated through a graded ethanol series, and infiltrated with Epon resin. Samples were processed by the Electron Microscopy Resource Laboratory at the Medical University of South Carolina using a Jeol Transmission Electron Microscope (JEM-1400Plus).

Electroretinography

Electroretinography recordings on mice were performed according to published procedures (45). Mice were dark-adapted overnight, anesthetized using xylazine (20 mg/kg) and ketamine (100 mg/kg), and pupils were dilated with 1 drop each of phenylephrine HCl (2.5%) and tropicamide (1%). Body temperature was stabilized via a DC-powered heating pad held at 37 °C. ERG recordings and data analyses were performed with the EPIC-4000 system (LKC Technologies, Inc.), using light stimuli with varying light intensities and wavelengths. Under scotopic conditions, responses to 10-μs single flashes of white light (maximum intensity of 2.48 photopic cd-s/m^2) between 40 and 0 db of attenuation were measured. After light-adapting animals for 8 min with rod-saturating light (35), UV-cone responses were tested using LED flashes centered at 360 nm at a single light intensity. Peak a-wave amplitude was measured from baseline to the initial negative-going voltage, whereas peak b-wave amplitude was measured from the trough of the a-wave to the peak of the positive b-wave.

Statistics

Results are presented as mean ± S.D. for image analysis and means ± S.E. of the mean for electroretinography. For pairwise comparisons, statistical significance was assessed using the two-tailed Student's *t* test. For ERG experiments, testing from the same animals over multiple light intensities and repeated measure ANOVA followed by Fisher's PLSD was used (StatView). For Western blot analysis, relative intensities of each band were quantified (densitometry) using ImageJ Software version 1.49 and normalized to the loading control.

Author contributions—J. H. L., G. P. L., and B. R. designed the research studies and wrote the manuscript. G. P. L., D. F., L. G., S. H. K., K. G., Y. S., E. O., Y. S., and X. Z. conducted experiments and acquired data. R. A. N., B. F., D. N., J. H. L., G. P. L., and B. R. analyzed and interpreted the data and reviewed the manuscript.

Acknowledgments—The UAB P30 Hepatorenal Fibrocystic Disease Core Center (supported by National Institutes of Health Grant P30DK074038) is gratefully acknowledged for generating the second exoc5 zebrafish mutant line using CRISPR gene editing, as well as for previously generating the Exoc5fl/fl mouse line.

References

1. Badano, J. L., Mitsuma, N., Beales, P. L., and Katsanis, N. (2006) The ciliopathies: an emerging class of human genetic disorders. *Annu. Rev. Genomics Hum. Genet.* **7,** 125–148
2. Bhogaraju, S., Engel, B. D., and Lorentzen, E. (2013) Intraflagellar transport complex structure and cargo interactions. *Cilia* **2,** 10
3. Cardenas-Rodriguez, M., and Badano, J. L. (2009) Ciliary biology: understanding the cellular and genetic basis of human ciliopathies. *Am. J. Med. Genet. C Semin. Med. Genet.* **151C,** 263–280

4. Baker, K., and Beales, P. L. (2009) Making sense of cilia in disease: the human ciliopathies. *Am. J. Med. Genet. C Semin. Med. Genet.* **151C,** 281–295
5. Blacque, O. E., and Leroux, M. R. (2006) Bardet-Biedl syndrome: an emerging pathomechanism of intracellular transport. *Cell. Mol. Life Sci.* **63,** 2145–2161
6. Smyth, B. J., Snyder, R. W., Balkovetz, D. F., and Lipschutz, J. H. (2003) Recent advances in the cell biology of polycystic kidney disease. *Int. Rev. Cytol.* **231,** 51–89
7. Bachmann-Gagescu, R., Phelps, I. G., Stearns, G., Link, B. A., Brockerhoff, S. E., Moens, C. B., and Doherty, D. (2011) The ciliopathy gene cc2d2a controls zebrafish photoreceptor outer segment development through a role in Rab8-dependent vesicle trafficking. *Hum. Mol. Genet.* **20,** 4041–4055
8. Baye, L. M., Patrinostro, X., Swaminathan, S., Beck, J. S., Zhang, Y., Stone, E. M., Sheffield, V. C., and Slusarski, D. C. (2011) The N-terminal region of centrosomal protein 290 (CEP290) restores vision in a zebrafish model of human blindness. *Hum. Mol. Genet.* **20,** 1467–1477
9. Luo, N., Lu, J., and Sun, Y. (2012) Evidence of a role of inositol polyphosphate 5-phosphatase INPP5E in cilia formation in zebrafish. *Vision Res.* **75,** 98–107
10. Sukumaran, S., and Perkins, B. D. (2009) Early defects in photoreceptor outer segment morphogenesis in zebrafish ift57, ift88, and ift172 intraflagellar transport mutants. *Vision Res.* **49,** 479–489
11. Besharse, J. C., Baker, S. A., Luby-Phelps, K., and Pazour, G. J. (2003) Photoreceptor intersegmental transport and retinal degeneration: a conserved pathway common to motile and sensory cilia. *Adv. Exp. Med. Biol.* **533,** 157–164
12. Liu, Q., Zhang, Q., and Pierce, E. A. (2010) Photoreceptor sensory cilia and inherited retinal degeneration. *Adv. Exp. Med. Biol.* **664,** 223–232
13. Tsujikawa, M., and Malicki, J. (2004) Genetics of photoreceptor development and function in zebrafish. *Int. J. Dev. Biol.* **48,** 925–934
14. Schmitt, E. A., and Dowling, J. E. (1999) Early retinal development in the zebrafish, *Danio rerio*: light and electron microscopic analyses. *J. Comp. Neurol.* **404,** 515–536
15. Branchek, T., and Bremiller, R. (1984) The development of photoreceptors in the zebrafish, *Brachydanio rerio*. I. Structure. *J. Comp. Neurol.* **224,** 107–115
16. Graw, J. (2010) Eye development. *Curr. Top. Dev. Biol.* **90,** 343–386
17. Deretic, D., Huber, L. A., Ransom, N., Mancini, M., Simons, K., and Papermaster, D. S. (1995) rab8 in retinal photoreceptors may participate in rhodopsin transport and in rod outer segment disk morphogenesis. *J. Cell Sci.* **108,** 215–224
18. Deretic, D., and Papermaster, D. S. (1993) Rab6 is associated with a compartment that transports rhodopsin from the trans-Golgi to the site of rod outer segment disk formation in frog retinal photoreceptors. *J. Cell Sci.* **106,** 803–813
19. Moritz, O. L., Tam, B. M., Hurd, L. L., Peränen, J., Deretic, D., and Papermaster, D. S. (2001) Mutant rab8 impairs docking and fusion of rhodopsin-bearing post-Golgi membranes and causes cell death of transgenic Xenopus rods. *Mol. Biol. Cell* **12,** 2341–2351
20. Nachury, M. V., Loktev, A. V., Zhang, Q., Westlake, C. J., Peränen, J., Merdes, A., Slusarski, D. C., Scheller, R. H., Bazan, J. F., Sheffield, V. C., and Jackson, P. K. (2007) A core complex of BBS proteins cooperates with the GTPase Rab8 to promote ciliary membrane biogenesis. *Cell* **129,** 1201–1213
21. Zuo, X., Guo, W., and Lipschutz, J. H. (2009) The exocyst protein Sec10 is necessary for primary ciliogenesis and cystogenesis *in vitro*. *Mol. Biol. Cell* **20,** 2522–2529
22. Zuo, X., Fogelgren, B., and Lipschutz, J. H. (2011) The small GTPase Cdc42 is necessary for primary ciliogenesis in renal tubular epithelial cells. *J. Biol. Chem.* **286,** 22469–22477
23. Fogelgren, B., Lin, S. Y., Zuo, X., Jaffe, K. M., Park, K. M., Reichert, R. J., Bell, P. D., Burdine, R. D., and Lipschutz, J. H. (2011) The exocyst protein Sec10 interacts with polycystin-2 and knockdown causes PKD-phenotypes. *PLoS Genet.* **7,** e1001361
24. Choi, S. Y., Chacon-Heszele, M. F., Huang, L., McKenna, S., Wilson, F. P., Zuo, X., and Lipschutz, J. H. (2013) Cdc42 deficiency causes ciliary abnormalities and cystic kidneys. *J. Am. Soc. Nephrol.* **24,** 1435–1450
25. Choi, S. Y., Baek, J. I., Zuo, X., Kim, S. H., Dunaief, J. L., and Lipschutz, J. H. (2015) Cdc42 and sec10 are required for normal retinal development in zebrafish. *Invest. Ophthalmol. Vis. Sci.* **56,** 3361–3370
26. Bizet, A. A., Becker-Heck, A., Ryan, R., Weber, K., Filhol, E., Krug, P., Halbritter, J., Delous, M., Lasbennes, M. C., Linghu, B., Oakeley, E. J., Zarhrate, M., Nitschké, P., Garfa-Traore, M., Serluca, F., et al. (2015) Mutations in TRAF3IP1/IFT54 reveal a new role for IFT proteins in microtubule stabilization. *Nat. Commun.* **6,** 8666
27. Stoetzel, C., Bär, S., De Craene, J. O., Scheidecker, S., Etard, C., Chicher, J., Reck, J. R., Perrault, I., Geoffroy, V., Chennen, K., Strähle, U., Hammann, P., Friant, S., and Dollfus, H. (2016) A mutation in VPS15 (PIK3R4) causes a ciliopathy and affects IFT20 release from the cis-Golgi. *Nat. Commun.* **7,** 13586
28. Badouel, C., Garg, A., and McNeill, H. (2009) Herding Hippos: regulating growth in flies and man. *Curr. Opin. Cell Biol.* **21,** 837–843
29. Happé, H., van der Wal, A. M., Leonhard, W. N., Kunnen, S. J., Breuning, M. H., de Heer, E., and Peters, D. J. (2011) Altered Hippo signalling in polycystic kidney disease. *J. Pathol.* **224,** 133–142
30. Liu, Q., Zuo, J., and Pierce, E. A. (2004) The retinitis pigmentosa 1 protein is a photoreceptor microtubule-associated protein. *J. Neurosci.* **24,** 6427–6436
31. Gargini, C., Terzibasi, E., Mazzoni, F., and Strettoi, E. (2007) Retinal organization in the retinal degeneration 10 (rd10) mutant mouse: a morphological and ERG study. *J. Comp. Neurol.* **500,** 222–238
32. Fogelgren, B., Polgar, N., Lui, V. H., Lee, A. J., Tamashiro, K. K., Napoli, J. A., Walton, C. B., Zuo, X., and Lipschutz, J. H. (2015) Urothelial defects from targeted inactivation of exocyst Sec10 in mice cause ureteropelvic junction obstructions. *PLoS ONE* **10,** e0129346
33. Aït-Ali, N., Fridlich, R., Millet-Puel, G., Clérin, E., Delalande, F., Jaillard, C., Blond, F., Perrocheau, L., Reichman, S., Byrne, L. C., Olivier-Bandini, A., Bellalou, J., Moyse, E., Bouillaud, F., Nicol, X., *et al.* (2015) Rod-derived cone viability factor promotes cone survival by stimulating aerobic glycolysis. *Cell* **161,** 817–832
34. Novick, P., and Guo, W. (2002) Ras family therapy: Rab, Rho and Ral talk to the exocyst. *Trends Cell Biol.* **12,** 247–249
35. Rogers, K. K., Wilson, P. D., Snyder, R. W., Zhang, X., Guo, W., Burrow, C. R., and Lipschutz, J. H. (2004) The exocyst localizes to the primary cilium in MDCK cells. *Biochem. Biophys. Res. Commun.* **319,** 138–143
36. Lechtreck, K. F., Johnson, E. C., Sakai, T., Cochran, D., Ballif, B. A., Rush, J., Pazour, G. J., Ikebe, M., and Witman, G. B. (2009) The *Chlamydomonas reinhardtii* BBSome is an IFT cargo required for export of specific signaling proteins from flagella. *J. Cell Biol.* **187,** 1117–1132
37. Dixon-Salazar, T. J., Silhavy, J. L., Udpa, N., Schroth, J., Bielas, S., Schaffer, A. E., Olvera, J., Bafna, V., Zaki, M. S., Abdel-Salam, G. H., Mansour, L. A., Selim, L., Abdel-Hadi, S., Marzouki, N., Ben-Omran, T., *et al.* (2012) Exome sequencing can improve diagnosis and alter patient management. *Sci. Transl. Med.* **4,** 138ra78
38. Shaheen, R., Faqeih, E., Alshammari, M. J., Swaid, A., Al-Gazali, L., Mardawi, E., Ansari, S., Sogaty, S., Seidahmed, M. Z., AlMotairi, M. I., Farra, C., Kurdi, W., Al-Rasheed, S., and Alkuraya, F. S. (2013) Genomic analysis of Meckel-Gruber syndrome in Arabs reveals marked genetic heterogeneity and novel candidate genes. *Eur. J. Hum. Genet.* **21,** 762–768
39. Meire, F., Delpierre, I., Brachet, C., Roulez, F., Van Nechel, C., Depasse, F., Christophe, C., Menten, B., and De Baere, E. (2011) Nonsyndromic bilateral and unilateral optic nerve aplasia: first familial occurrence and potential implication of CYP26A1 and CYP26C1 genes. *Mol. Vis.* **17,** 2072–2079
40. Frühmesser, A., Blake, J., Haberlandt, E., Baying, B., Raeder, B., Runz, H., Spreiz, A., Fauth, C., Benes, V., Utermann, G., Zschocke, J., and Kotzot, D. (2013) Disruption of EXOC6B in a patient with developmental delay, epilepsy, and a de novo balanced t(2;8) translocation. *Eur. J. Hum. Genet.* **21,** 1177–1180
41. Wen, J., Lopes, F., Soares, G., Farrell, S. A., Nelson, C., Qiao, Y., Martell, S., Badukke, C., Bessa, C., Ylstra, B., Lewis, S., Isoherranen, N., Maciel, P., and Rajcan-Separovic, E. (2013) Phenotypic and functional consequences of

haploinsufficiency of genes from exocyst and retinoic acid pathway due to a recurrent microdeletion of 2p13.2. Orphanet. *J. Rare Dis.* **8,** 100

42. Seixas, C., Choi, S. Y., Polgar, N., Umberger, N. L., East, M. P., Zuo, X., Moreiras, H., Ghossoub, R., Benmerah, A., Kahn, R. A., Fogelgren, B., Caspary, T., Lipschutz, J. H., and Barral, D. C. (2016) Arl13b and the exocyst interact synergistically in ciliogenesis. *Mol. Biol. Cell* **27,** 308–320
43. Johnson, R., and Halder, G. (2014) The two faces of Hippo: targeting the Hippo pathway for regenerative medicine and cancer treatment. *Nat. Rev. Drug Discov.* **13,** 63–79
44. Luna, G., Lewis, G. P., Linberg, K. A., Chang, B., Hu, Q., Munson, P. J., Maminishkis, A., Miller, S. S., and Fisher, S. K. (2016) *An*atomical and gene expression changes in the retinal pigmented epithelium atrophy 1 (rpea1) Mouse: a potential model of serous retinal detachment. *Invest. Ophthalmol. Vis. Sci.* **57,** 4641–4654
45. Woodell, A., Coughlin, B., Kunchithapautham, K., Casey, S., Williamson, T., Ferrell, W. D., Atkinson, C., Jones, B. W., and Rohrer, B. (2013) Alternative complement pathway deficiency ameliorates chronic smoke-induced functional and morphological ocular injury. *PLoS ONE,* **8,** e67894